A DSP Based Indirect Field-Oriented Induction Motor Position and Speed Control System

Paulo R. M. Costa [*] **Marcus R. de Castro** [**] **Isaac R. Machado** [***]
Tárcio A. d. S. Barros [****]

[*] *Electrical Engineering Course, Sobral's Campus, Federal University of Ceará, CE, (e-mail: robsoncee@gmail.com).*
[**] *Electrical Engineering Course, Sobral's Campus, Federal University of Ceará, CE, (e-mail: marcusdecastro@yahoo.com.br).*
[***] *Electrical Engineering Course, Sobral's Campus, Federal University of Ceará, CE, (e-mail: isaacmachado@ufc.br).*
[****] *Faculdade de Engenharia Mecânica, Universidade Estadual de Campinas, SP, (e-mail: tarcioandre@fem.unicamp.br)*

Abstract: Due to the three-phase induction machines (TIM) operation principle, the position control of this kind of motor is not trivial. Advances in power electronics, microprocessors technological improvements, and new control strategies have favored TIM control applications, increasingly more precise results. Position control allows the application of TIM in robotic manipulators, for example, replacing the more expensive DC machine. Thus, a Three-phase induction machine position control by indirect field-oriented strategy based on a back-to-back topology converter and Digital Signal Processor (DSP) is presented in this paper. An incremental encoder was used to obtain the angular position of the machine's rotor. Proportional-Integral controllers were used in the position and speed control loops. Due to the high sampling frequency achieved (200 kHz), a hysteresis current controller was used. The experimental results obtained validated the adopted strategies.

Keywords: three-phase induction machines (TIM); Digital Signal Processor (DSP); position control; speed control; Proportional-Integral; hysteresis current controller.

1. INTRODUCTION

The industrial automation process is increasingly demanding the application of electric motors, requiring torque, speed, or position control. The advancement of power electronics, especially the emergence of IGBT in the mid-1980s, and microprocessors, as well as their cheapness, allowed inverters to become cheaper and capable of computing complex modeling, and the control of induction motors became viable. Squirrel-cage induction motors represent the majority of motors sold in Brazil and are responsible for a considerable part of the electrical energy consumed. This highlights the importance of ongoing studies on efficiency and control for advanced applications of this equipment.

Employing Clark and Park's transforms, the TIM electrical model in *abc* reference frame can be rewritten in synchronous *dq* reference frame. The field-oriented control is based on concentrating the entire rotor field flux on the synchronous reference frame direct axis. Thus, it is possible to control flux and torque by uncoupled currents, similar to the control of direct current machines. Since the field-oriented control system is indirect, the position of the rotor field flux is not directly measured but estimated. Assuming that the flux is aligned on the direct axis, the control system indirectly imposes the flux alignment (Ong, 1998).

Several strategies were adopted to control the TIM. We can point out some approaches present in the literature: Predictive Current Control was used by R and M (2015), speed and current controllers based on fuzzy logic (Fahassa et al., 2015; Zhen and Xu, 2000), fuzzy-PI speed controller (Magzoub et al., 2013; Hannan et al., 2018), modified indirect field-oriented control (MIFOC) (Nishad and Sharma, 2018), Imperialist Competitive Algorithm (ICA)-optimized PI speed control (Razavi and Ghadiri, 2011), on-line parameter estimation using the steady-state voltage model based rotor flux observation (Zhang et al., 2014), adaptive Sliding Mode Control (SMC) for speed control (Patakor et al., 2011) and Space Vector Modulation (Hiware and Chaudhari, 2011).

This work presents a DSP strategy to control the three-phase induction machine based on indirect field-oriented control. Experimental results of a TIM's position and speed control validated the proposed control strategy. This work aims to promote the possibility of realizing position control in many applications using the TIM and be a starting point for studying more advanced control techniques to improve the system's dynamic performance and efficiency.

The paper is organized as follows: Section 2 describes the motor model which is necessary to realize the control, Section 3 presents the control strategy adopted, while the main experimental results are shown in Section 4.
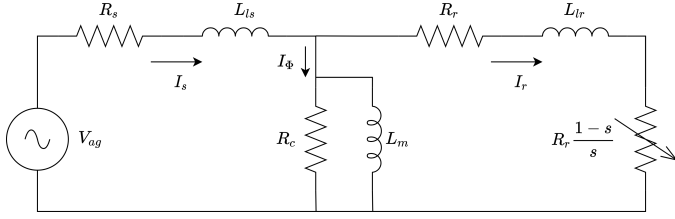
Figure 1. Steady-state per phase model of an induction machine

2. MODELING

The electrical transient is negligible in the per-phase equivalent circuit of the induction machine, shown in Figure 1. The model expresses the per-phase equivalent wye connection of the machine in steady-state, and it is helpful to obtain the machine parameters through no-load and rotor-blocked tests. Getting these parameters is essential for Indirect Field-Oriented based control. Phase windings are considered identical and the voltages and currents are purely sinusoidal. The motor magnetic material is assumed to be linear and all the parameters are stator side referred. The stator and rotor copper losses are represented by R_s and R_r, respectively. L_{ls} and L_{lr} are stator and rotor the leakage inductances, while L_m is the magnetizing inductance. The R_c resistor represents the core losses. The element $R_r(1-s)/s$ expresses the mechanical output power (Umans et al., 2013).

Due to the complexity of the TIM model in abc reference frame, some mathematical manipulations, such as the Clark and Park transforms, are used to obtain a simpler model. The Clarke transformation ou $\alpha\beta 0$ transformation decomposes the system vector in two stationary square axes, α and β axes, keeping equivalent torque, power and speed. Park transformation converts the three-phase symmetric machine into a two-phase symmetric machine, decomposed into two quadrature axes, the direct axis (d) and the quadrature axis (q) rotating at a certain speed (Umans et al., 2013; Barbi, 1985). In this work, we consider the synchronous dq coordinate system, as it rotates at the synchronous frequency of the supply voltages.

The model of the induction motor in synchronous dq reference frame system can be found at Reginatto (1993); Barbi (1985); Ong (1998).

The synchronous dq reference frame model of the induction motor can be written as follows (Reginatto, 1993). For the stator voltages:

$$v_{qs} = R_s i_{qs} + p\lambda_{qs} + \omega_e \lambda_{ds} \tag{1}$$
$$v_{ds} = R_s i_{ds} + p\lambda_{ds} + \omega_e \lambda_{qs} \tag{2}$$

where, v, i, and λ are voltage, current and flux linkage, respectively. The d and q subscribed indicate the axis from the qd coordinates system. The s subscribed denotes that the variables are from the stator. ω_e is the synchronous electrical angular speed. p is the time derivative operator.

The rotor voltages are zero, so we can write:

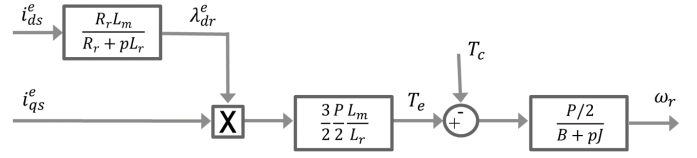$$0 = R_r i_{qr} + p\lambda_{qr} + (\omega_e - \omega_r)\lambda_{dr} \tag{3}$$

Figure 2. Flux oriented TIM model.

$$0 = R_r i_{dr} + p\lambda_{dr} + (\omega_e - \omega_r)\lambda_{qr} \tag{4}$$

where r subscribed denotes the variables from the rotor. The ω_r is the mechanical angular speed of the rotor.

The equations for the stator and rotor flux linkages on the d and q axes are:

$$\lambda_{qs} = L_s i_{qs} + L_m i_{qr} \tag{5}$$
$$\lambda_{ds} = L_s i_{ds} + L_m i_{dr} \tag{6}$$
$$\lambda_{qr} = L_r i_{qr} + L_m i_{qs} \tag{7}$$
$$\lambda_{dr} = L_r i_{dr} + L_m i_{ds} \tag{8}$$

where L_s and L_r are the self-inductances of the stator and rotor, and L_{srm} is the stator and rotor mutual inductance.

The eletromagnetic torque (T_e) is calculated by:

$$T_e = \frac{3}{2}\frac{P}{2}\frac{L_m}{L_r}(\lambda_{dr} i_{qs} - \lambda_{qr} i_{ds}) \tag{9}$$

where P is the number of stator poles.

The mechanical dynamic is described by:

$$\frac{P}{2}(T_e - T_l) = p\omega_r J + \omega B \tag{10}$$

where T_l is the load torque, J is the moment of inertia, and B friction coefficient.

The orientation of the rotor field flux consists of aligning the flux vector λ_r along the d axis (λ_{dr}) in such a way that it can be written: $\lambda_{dr} = \lambda_r$ and $\lambda_{qr} = p\lambda_{qr} = 0$. Where p is the time derivative operator. The fact that the quadrature component of the rotor flux (λ_{qr}) is null establishes a direct relationship between the quadrature components of the stator and rotor currents. Developing the equations of the induction motor model in the synchronous axis system, considering the rotor quadrature flux equal to zero, we have:

$$\lambda_r = \lambda_{dr} = \frac{L_m R_r}{pL_r + R_r} i_{ds} \tag{11}$$

where L_m is the mutual inductance of the windings, L_r is the self-inductance of the rotor winding, R_r is the electrical resistance of the rotor winding, and i_{ds} is the d axis component of the stator current.

After concentrating the linkage flux in the d axis, the electromagnetic torque equation becomes:

$$T_e = \frac{3}{2}\frac{P}{2}\frac{L_m}{L_r}(\lambda_{dr} i_{qs}). \tag{12}$$
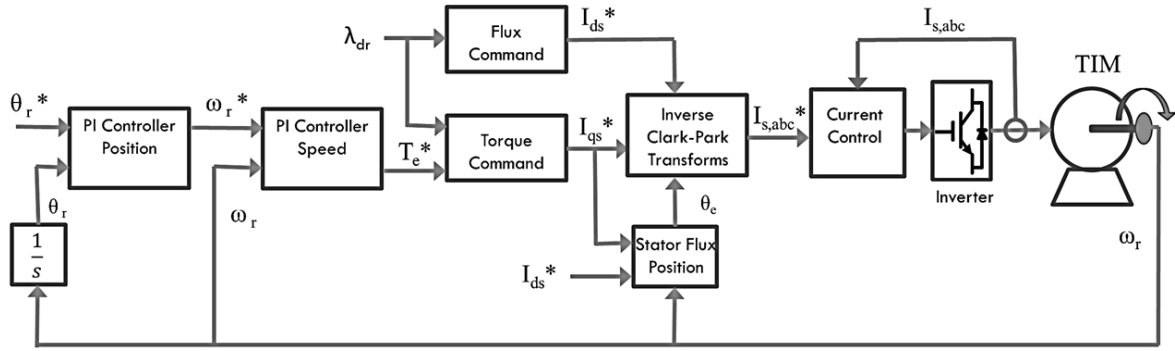
Figure 3. Schematic diagram of position control by indirect field-oriented.

The equations above determine the behavior of the torque and the motor flux when the rotor flux is oriented along the direct axis, see Figure 2. These equations show that: the flux $\lambda_{dr} = \lambda_r$, depends solely on the component i_{ds} of the stator current; if the flux λ_{dr} is constant, the electromagnetic torque is proportional to the component i_{qs}. This means that the stator current components d and q have been decoupled in the components that produce flux and torque in the motor, respectively. For this case, the following expression provides the angular slip speed (ω_2):

$$\omega_2 = \omega_e - \omega_r = \frac{R_r}{L_r}\frac{i_{qs}}{i_{ds}} \qquad (13)$$

The synchronization angle or angle of the stator magnetic field (θ_e) can be estimated by:

$$\theta_e = \theta_r + \int \omega_2(t)dt = \int \omega_r(t)dt + \int \omega_2(t)dt, \qquad (14)$$

where θ_r it is the angular rotor position and can be obtained directly by an absolute encoder or from the speed ω_r obtained by an incremental encoder and integrated into time (Shrawane, 2010).

3. CONTROL STRATEGIES

Based on the model obtained in equations (11) and (12), it is possible to control the speed and position of the induction motor. Figure 3 shows the block diagram of the position control system. Proportional-Integral (PI) controllers were used to control the position speed and loops (outer loops). For the current control (inner loop), a hysteresis controller was used.

Getting the position command (θ_r^*) and the actual position (θ_r), the PI position controller generates the speed command (ω_r^*). For speed control, ω_r^* is defined directly. The PI speed controller output is the torque command (T_e^*). The stator quadrature current command (I_{qs}^*) is calculated by the *Torque Command* block shown on Figure 4. The stator direct current command (I_{ds}^*) is calculated by the *Flux Command* block shown on Figure 5. The TIM obtained model is used to estimate the electrical angle of the flux (θ_e) by the *Stator Flux Position* block, shown in Figure 6. Then, the stator command currents $(I_{ds}^*$ and $I_{qs}^*)$ are calculated and transformed into *abc* reference frame (I_{abc}^*). The
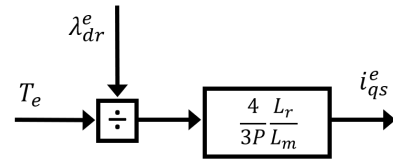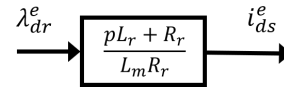

Figure 4. Torque command block.
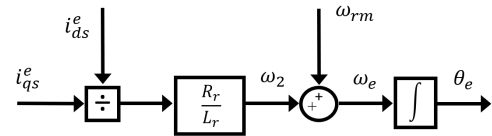

Figure 5. Flux command block.

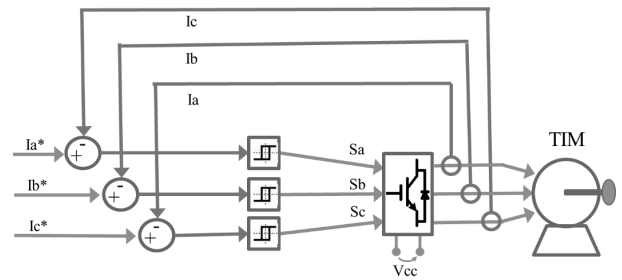Figure 6. Stator flux position estimator block.

Figure 7. Hysteresis current controller.

current controller, Figure 7, compares the actual measured current with the commands and generates the switching pulses for the inverter.

The main advantages of hysteresis current controllers are simplicity, robustness, excellent dynamic performance, and independence of load parameters. The disadvantages of this type of control are sampling frequency limitation, variable switching frequency, and dependent on the time constant of the load and the source voltage.

The three-phase supply, rectifier, DC bus, inverter, and motor set are represented in Figure 8.
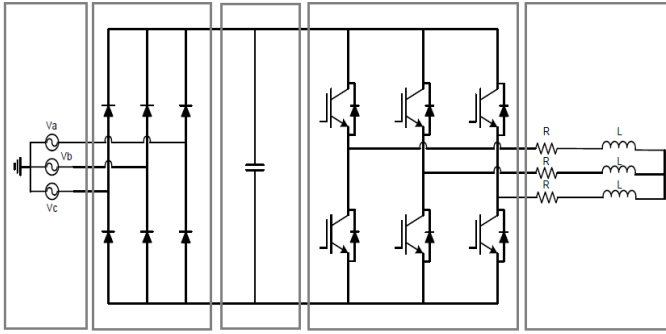
Figure 8. Inverter circuit.

3.1 Transfer functions for tuning controllers

From the motor model obtained, it is possible to deduce the transfer functions needed to tune the controllers. It is known that $\omega = d\theta/dt$, so the transfer function for the position control loop is

$$G_\theta(s) = \frac{\theta_r(s)}{\omega_r(s)} = \frac{1}{s}. \tag{15}$$

From the equation (10), the transfer function for the speed control loop can be written as

$$G_\omega(s) = \frac{\omega_r(s)}{T_e(s)} = \frac{1/J}{s + B/J}. \tag{16}$$

The transfer function for the current loop dynamics in dq reference frame is (Barbi, 1985):

$$G_{i_d}(s) = \frac{i_{ds}(s)}{v_{ds}(s)} = \frac{\frac{1}{L_s\sigma}}{s + \left(\frac{R_s}{L_s\sigma} + \frac{1-\sigma}{\delta_r\sigma}\right)}. \tag{17}$$

Despite using hysteresis current controller in abc reference frame, the equation (17) helps tune a linear controller that could be employed for current control.

4. EXPERIMENTAL RESULTS

To validate the vector control experimentally, the converter shown in Figure 9 was used, as well as the motor, Foucault brake, and encoder assembly shown in Figure 10. This bench comprises two three-phase converters with a shared DC link, known as *back-to-back*. The inverter switches are 15 A IGBT, and the DC bus is limited to 450 V. The control board is the *Texas Instruments* CCTI335 and is controlled by the TI F28335 DSP. As in our application the induction machine is used only as a motor, converter 2 (CONV2) was used only as a three-phase rectifier, receiving the three-phase voltages from the network and delivering DC voltage to the DC link. A pre-charge circuit for current-limited initial charging of capacitors is also provided. For the current measurement, LEM HXS 20-NP Hall effect sensors were used. For measuring speed and position, the incremental and bidirectional encoder 59C (2500 pulses per revolution) was used. Table 1 presents all the electrical and mechanical parameters of the 1 hp TIM, as the digital controllers' parameters.
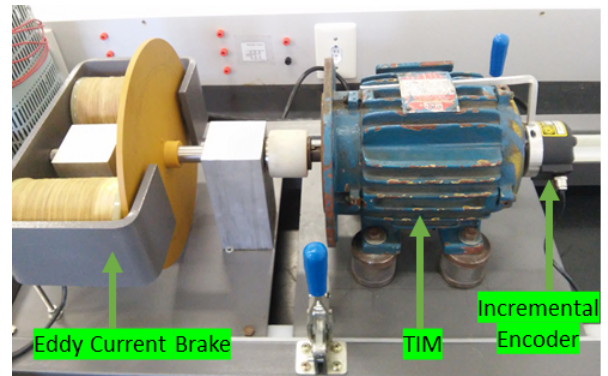

Figure 9. Converter bench

Figure 10. Motor, eddy current brake and encoder assembly.

Figure 11 shows the flowchart of the program implemented to perform vector control. As seen in the flowchart, the program has three interrupts in order of highest priority. The first one occurs when there is a rising edge in the signal coming from the *encoder*. The second occurs when the *timer1* counter reaches 5 ms and the third occurs when

Table 1. Motor and controller parameters.

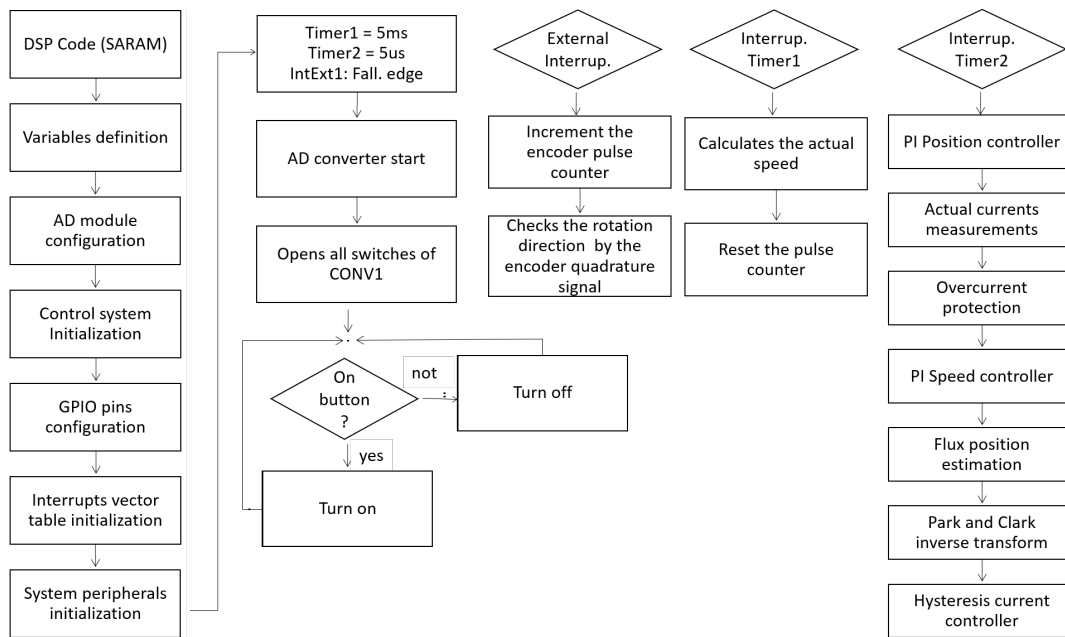| Parameter	Value
R_s (Ω)	5.350
R_r (Ω)	11.74
X_{ls} (Ω)	23.64
X_{lr} (Ω)	14.15
X_m (Ω)	122.8
L_m (H)	0.326
L_s (H)	0.388
L_r (H)	0.363
δ_r (s)	0.031
σ	0.248
J ($kg \cdot m^3$)	0.013
B ($N \cdot m \cdot s$)	2.598×10^{-3}
$T_{s,\omega}$ (s)	5×10^{-6}
$Kp_{z,\omega}$	2.575
$Ki_{z,\omega}$	1.612×10^{-4}
$T_{s,\theta}$ (s)	5×10^{-5}
$Kp_{z,\theta}$	64
$Ki_{z,\theta}$	1.6×10^{-4}
P	4
i_{ds}	1.8 A
λ_{dr}	0.586 Wb

Figure 11. Program flowchart implemented in DSP.
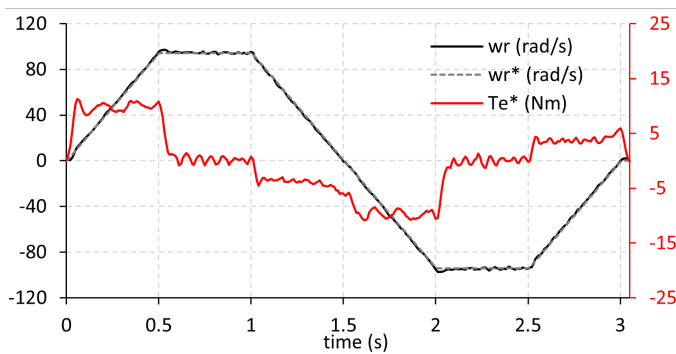

Figure 12. Rotor angular speed (wr), Rotor angular speed command (wr*) and electromagnetic torque command (Te*) in the no-load speed test
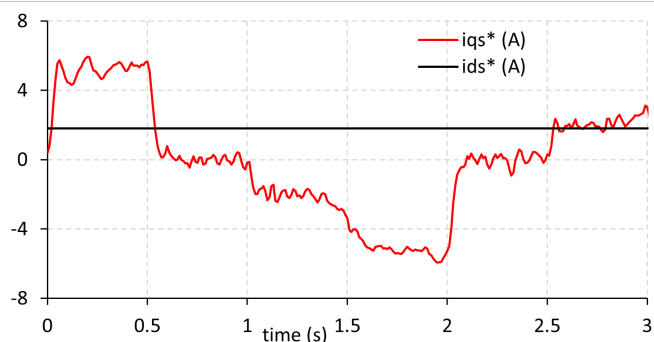

Figure 13. Currents commands i_{ds}^* and i_{qs}^* in the no-load speed test.

the *timer2* counter reaches 5 μs. As in vector control the acquisition and current control occur at the interruption of *timer2*, the program sampling time is 5 μs, implying a sampling frequency of 200 kHz.
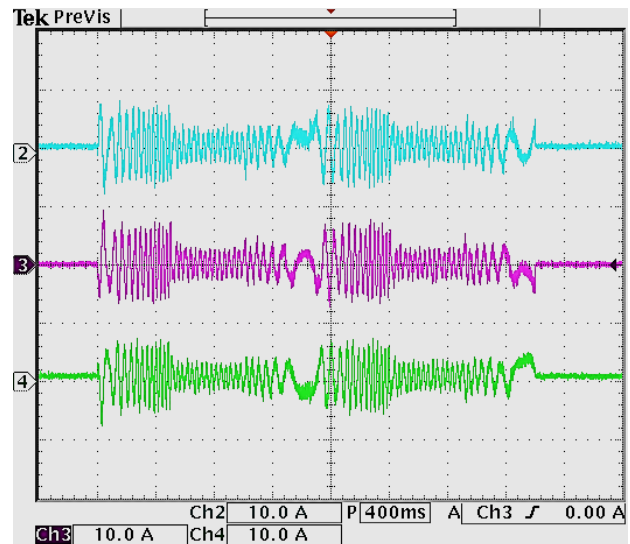

Figure 14. Three-phase line currents in the no-load speed test.

To validate the adopted strategies, experimental results for TIM's speed and position control are shown.

4.1 No-load speed control test

The experimental result for the speed control of the induction motor shaft using vector control according to the work cycle of the speed test with inversion of direction is presented in Figure 12, 13 e 14. The largest errors in speed control occurred when there was variation in acceleration, reaching an error of 3,016 rad/s (3.20%), and the maximum setting time by the 2 % criterion was 0.05 seconds. The average error during the test was around 0.83%. It is observed that the reference electromagnetic torque, the output of the PI speed controller, is maximum
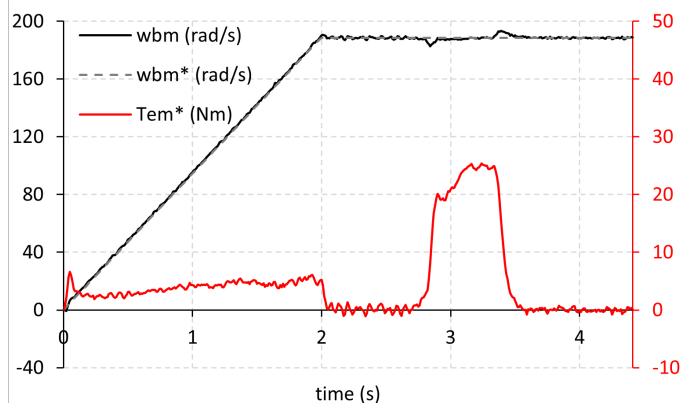
Figure 15. Rotor speed (wbm), reference speed (wbm*) and reference electromagnetic torque (Tem*) in the loaded speed test.
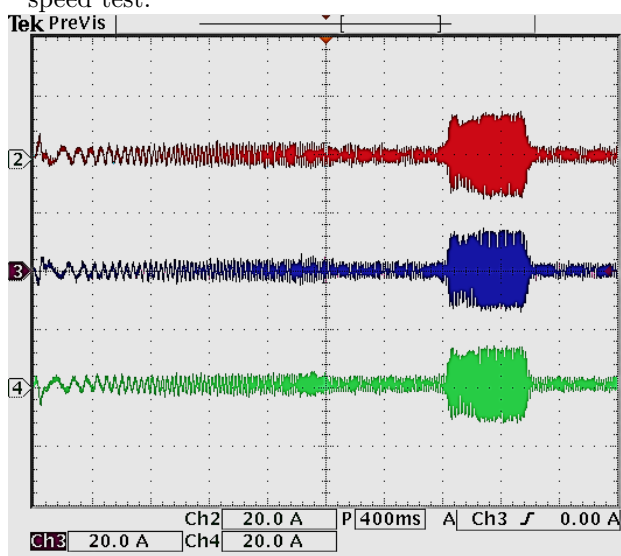

Figure 16. Three-phase line currents in the loaded speed test.

at times of positive acceleration and has a low mean value at times of constant speed. It can be seen how the direct and quadrature axis reference currents behaved during activation in Figure 13. We see that the direct axis current (i_{ds}^*) responsible for the flux remains constant while the quadrature current takes on values to compensate for the speed error with electromagnetic torque. The three measured stator line currents are shown in Figure 14, and the amplitude and frequency of the currents can be observed.

4.2 Loaded speed control test

The experimental result for the speed control of the induction motor using vector control according to the test duty cycle with load application is presented in Figures 15 and 16. An eddy brake was used to apply mechanical load to the motor shaft. In Figure 15, we see that the rotor speed followed the reference during the starting ramp and the load entry and exit. The most significant errors occurred during load disturbances, reaching an overshoot of 4.90 rad/s (2.60%) at the time of load removal. The settling time by the 2% criterion was 0.07
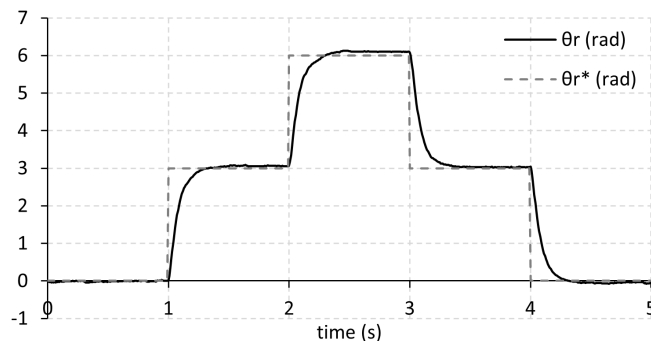

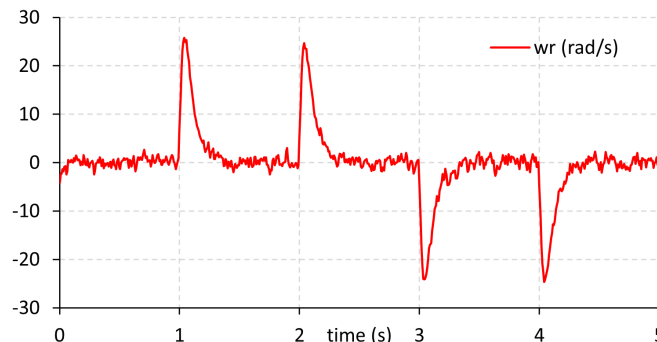Figure 17. Motor shaft position (θ_r) and position command (θ_r*).

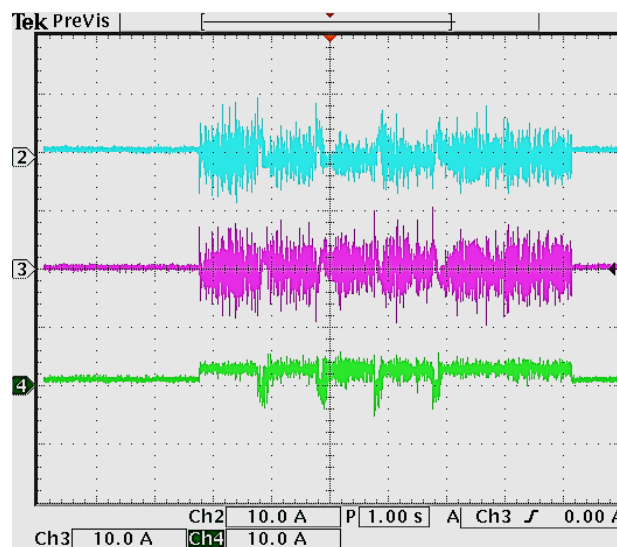Figure 18. Rotor speed (wr) during the position control test.

Figure 19. Three-phase line currents in the position control test.

s. The average error during the entire test was 0.92%. During start-up, there is positive electromagnetic torque due to acceleration. The reference electromagnetic torque is maximum when the load is applied and is minimum at times of constant reference speed and without load. The current is composed almost only of the direct axis component in this interval.

4.3 Position control test

The experimental result for the position control of the motor shaft using vector control according to the work cycle

for the position control test is presented in Figure 17, 18 and 19. In Figure 17, it can be seen that the rotor position followed the positive and negative command steps. The most significant error during steady state was 1.69% (0.1 rad), and the settling time for the 2 % criterion was 272 ms. The speed behavior during the position control test can be seen in Figure 18. The three stator line currents are shown in Figure 19.

5. CONCLUSION

The main objective of this work was to present a strategy to control the position and speed of the three-phase induction motor. The model used allowed to control of the motor's flux and torque by decoupled currents. The applications of position and speed control are as varied as possible in the industry, automobiles, robotics, and other sectors. The electrical and mechanical parameters obtained through tests and the gains of the controllers designed by pole allocation proved valid by analyzing the experimental results. A steady state error in some tests can be caused by inaccurate machine parameters and interference from the noise produced by the high-frequency switching of the IGBT of the converter, affecting the measurements of the currents and the encoder signals. It is also noted that, in position control, the TIM can lose its self-ventilation capacity. It is necessary to observe the temperature in the windings.

REFERENCES

Barbi, I. (1985). *Teoria fundamental do motor de induçao*. Série Didáctica. Editora da UFSC/Electrobrás. URL `https://books.google.com.br/books?id=hz3ZGwAACAAJ`.

Fahassa, C., Sayouti, Y., and Akherraz, M. (2015). Improvement of the induction motor drive's indirect field oriented control performance by substituting its speed and current controllers with fuzzy logic components. In *2015 3rd International Renewable and Sustainable Energy Conference (IRSEC)*, 1–6. doi:10.1109/IRSEC. 2015.7454928.

Hannan, M.A., Ali, J.A., Mohamed, A., Amiruld-din, U.A.U., Tan, N.M.L., and Uddin, M.N. (2018). Quantum-behaved lightning search algorithm to improve indirect field-oriented fuzzy-pi control for im drive. *IEEE Transactions on Industry Applications*, 54(4), 3793–3805. doi:10.1109/TIA.2018.2821644.

Hiware, R.S. and Chaudhari, J. (2011). Indirect field oriented control for induction motor. In *2011 Fourth International Conference on Emerging Trends in Engineering Technology*, 191–194. doi:10.1109/ICETET.2011.56.

Magzoub, M.A., Saad, N.B., and Ibrahim, R.B. (2013). An intelligent speed controller for indirect field-oriented controlled induction motor drives. In *2013 IEEE Conference on Clean Energy and Technology (CEAT)*, 327–331. doi:10.1109/CEAT.2013.6775650.

Nishad, B.K. and Sharma, R. (2018). Induction motor control using modified indirect field oriented control. In *2018 8th IEEE India International Conference on Power Electronics (IICPE)*, 1–5. doi:10.1109/IICPE. 2018.8709426.

Ong, C. (1998). *Dynamic Simulation of Electric Machinery: Using MATLAB/SIMULINK*. Prentice Hall PTR. URL `https://books.google.com.br/books?id=\_OweAQAAIAAJ`.

Patakor, F.A., Sulaiman, M., and Ibrahim, Z. (2011). Adaptive sliding mode for indirect field oriented controlled of induction motor. In *2011 IEEE Student Conference on Research and Development*, 289–293. doi: 10.1109/SCOReD.2011.6148752.

R, A.K.G. and M, W.B. (2015). Indirect field oriented control of induction motor using predictive current controller. In *2015 International Conference on Control Communication Computing India (ICCC)*, 248–253. doi: 10.1109/ICCC.2015.7432900.

Razavi, F. and Ghadiri, B. (2011). Imperialist competitive algorithm (ica)-optimized pi speed control in the indirect field-oriented control of an im drive. In *2011 IEEE Colloquium on Humanities, Science and Engineering*, 445–448. doi:10.1109/CHUSER.2011.6163770.

Reginatto, R. (1993). Controle por campo orientado do motor de indução com adaptação de parametros via mrac.

Shrawane, P. (2010). Indirect field - oriented control of induction motor. In *12th IEEE International Power Electronics Congress*, 102–105. doi:10.1109/CIEP.2010. 5598838.

Umans, S., Fitzgerald, A., and Kingsley, C. (2013). *Electric Machinery: Seventh Edition*. McGraw-Hill Higher Education. URL `https://books.google.com.br/books?id=dZkfAAAAQBAJ`.

Zhang, J., Chai, J., Sun, X., and Lu, H. (2014). On-line parameter estimation for indirect field oriented control of induction machine based on steady state voltage model. In *IECON 2014 - 40th Annual Conference of the IEEE Industrial Electronics Society*, 769–773. doi: 10.1109/IECON.2014.7048587.

Zhen, L. and Xu, L. (2000). Fuzzy learning enhanced speed control of an indirect field-oriented induction machine drive. *IEEE Transactions on Control Systems Technology*, 8(2), 270–278. doi:10.1109/87.826798.